

Ferroelectricity enhancement in confined nanorods: Direct variational method

Anna N. Morozovska*

*V. Lashkaryov Institute of Semiconductor Physics, NAS of Ukraine, 41, pr. Nauki, 03028 Kiev, Ukraine*Eugene A. Eliseev[†] and Maya D. Glinchuk[‡]*Institute for Problems of Materials Science, NAS of Ukraine, Krjijanovskogo 3, 03142 Kiev, Ukraine*

(Received 22 March 2006; revised manuscript received 21 April 2006; published 7 June 2006)

Ferroelectric nanoparticles of different shapes and their nanocomposites are actively studied by modern physics. Because of their applications in many fields of nanotechnology, the size effects and the possible disappearance of ferroelectricity at a critical particle volume attract a growing scientific interest. In this paper we study the size effects of the cylindrical nanoparticle phase diagrams allowing for effective surface tension and depolarization field influence. The Euler-Lagrange equations were solved by the direct variational method. The approximate analytical expression for the paraelectric-ferroelectric transition temperature dependence on nanoparticle sizes, polarization gradient coefficient, extrapolation length, effective surface, tension and electrostriction coefficient was derived. It was shown that the transition temperature could be higher than the one of the bulk material for nanorods and nanowires in contrast to nanodisks, where the decrease appears. We show that among all cylindrical shapes a nanobar reveals the minimal critical volume. Therefore we predict conservation and enhancement of ferroelectric properties in nanorods and nanowires. Obtained results explain the observed ferroelectricity enhancement in nanorods and could be very useful for the elaboration of modern nanocomposites with perfect polar properties.

DOI: [10.1103/PhysRevB.73.214106](https://doi.org/10.1103/PhysRevB.73.214106)

PACS number(s): 77.80.-e, 77.84.Dy, 68.03.Cd, 68.35.Gy

I. INTRODUCTION

Ferroelectric nanoparticles of different shape are actively studied in nanophysics and nano-technology. Because of miniaturization of devices based on these materials, the study of ferroelectric properties size dependence and the possible disappearance of ferroelectricity at a finite critical volume attract great interest.

The ferroelectric phase was studied in ferroelectric nanowires, nanotubes, and nanorods.¹⁻⁵ It appears that nanorods and nanotubes possess such polar properties as remnant polarization¹ and piezoelectric hysteresis.^{4,5,3} Moreover, so-called “confined” geometry does not destroy the ferroelectric phase as predicted for spherical particles^{6,7} and observed experimentally,⁸⁻¹⁰ but sometimes the noticeable enhancement of ferroelectric properties appears in nanocylinders.^{1-5,11}

Yadlovker and Berger¹ reported on the spontaneous polarization enhancement up to $0.25-2 \mu\text{C}/\text{cm}^2$ and ferroelectric phase conservation in Roshelle salt (RS) nanorods (radius about 30 nm and height 500 nm) up to the material decomposition temperature 55°C that is about 30°C higher than the one of bulk-size crystals.

Mishina *et al.*¹¹ revealed that ferroelectric phase exists in $\text{PbZr}_{0.52}\text{Ti}_{0.48}\text{O}_3$ (PZT) nanorods with diameters less than 10–20 nm. However, earlier Mishra and Pandey⁹ demonstrated that the ceramics prepared from the powders of $\text{PbZr}_{0.52}\text{Ti}_{0.48}\text{O}_3$ with a size about 100 nm had a pseudocubic symmetry, but might exhibit a hump in the temperature variation of dielectric constant. So, it seems that the critical size for the PZT nanorod (if any) is about ten times smaller than the one for the nanosphere.

Geneste *et al.*² studied the size dependence of the ferroelectric properties of BaTiO_3 (BT) nanowires from

the first principles. They showed that the ferroelectric distortion along the wire axis disappears below a critical size of about 1.2 nm, also it can be recovered under the appropriate strain conditions. Note, that BaTiO_3 spherical nanoparticles have the much longer critical diameter of about 100 nm.¹⁰

Morrison *et al.*⁵ demonstrated that ultra-small $\text{PbZr}_{0.52}\text{Ti}_{0.48}\text{O}_3$ nanorods and nanotubes (radius $R=20-30$ nm, length $50 \mu\text{m}$) possesses a rectangular shape of the piezoelectric hysteresis loop with an effective remnant piezoelectric coefficient value compatible with the ones typical for PZT films.¹² This fact unambiguously speaks in favor of spontaneous polarization existence. Also the authors demonstrated that the ferroelectric properties of the free BaTiO_3 nanotubes are perfect.

Thus, at first glance, recent experimental results contradict the generally accepted viewpoint that the ferroelectric properties disappear under the system volume decreases below the critical one.¹³ Actually the aforementioned facts proved that the shape of nanoparticles (e.g., the spherical or cylindrical one) essentially influences the critical volume necessary for the ferroelectricity conservation² possibly owing to the different depolarization field and mechanical boundary conditions.^{14,15} Immediately one should ask the principal question: “What nanoparticle shape possesses the minimal critical volume and allows ferroelectricity conservation at higher temperatures? Could the answer be predicted theoretically?”

In theoretical papers,^{6,16} special attention was paid to size effects, but depolarization field influence on a nanoparticle was neglected. However, it is well known that the depolarization field exists in the majority of confined ferroelectric systems¹⁷ and causes the aforementioned size-induced ferroelectricity disappearance in insulator single-domain films

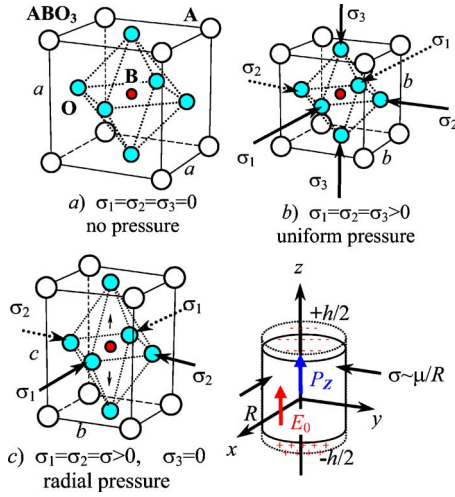


FIG. 1. (Color online) The perovskite cubic unit cell (a), its compression under the uniform (hydrostatic) pressure (b) only clamps the B-site cation in the centrosymmetrical position (i.e., stabilizes the paraelectric cubic phase). The lateral pressure (c) induces the transition of cubic unit cell into the nonpolar tetragonal one (the lowering of symmetry stimulates the ferroelectric phase appearance at higher temperatures).

and ellipsoidal particles.^{18–20} Both finite size and depolarization field effects lead to the ferroelectric properties degradation, namely, the phase transition temperature in spherical nanoparticles is significantly lower than the bulk one for most of the cases.^{6,21,20,8}

In this paper we study the size effects, surface tension, and depolarization field influence on the noninteracting nanoparticles assembly. We suppose that a nanoparticle surface is covered with a charged layer consisting of the free carriers adsorbed in the ambient conditions (e.g., air with definite humidity or pores filled with a precursor water solution). For instance, a thin water layer condensates on the polar oxide surface in the air with humidity 20–50%.²² The surface charges screen the surrounding medium from the nanoparticle electric field,¹³ but the depolarization field inside the particle is caused by inhomogeneous polarization distribution. Thus we calculated the depolarization field inside a cylindrical nanoparticle under the short-circuit conditions proposed by Kretschmer and Binder.¹⁸

For the description of nanodisks, nanorods, and nanowires ferroelectric properties we used the Euler-Lagrange equations solved by means of a direct variational method.¹⁹ The approximate analytical expression for paraelectric-ferroelectric transition temperature dependence on the nanoparticle sizes, extrapolation length, effective surface tension coefficient, polarization gradient, and electrostriction coupling coefficients, *etc.*, was derived. We obtained that the possible reason of the polar properties enhancement in confined ferroelectric nanowires and nanorods is the radial pressure caused by the effective surface tension and coupled with a polarization via electrostriction effect.

It was shown earlier that the phase transition temperature increase takes place in the epitaxial films of perovskite fer-

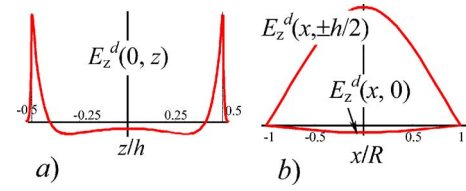


FIG. 2. (Color online) The depolarization field cross-sections $x=0$ (a) and $z=0; \pm h/2$ (b).

roelectrics due to the misfit strain between film and its substrate.¹⁴ However, for the bulk ferroelectrics the hydrostatic pressure (uniform compression) has a different effect on the phase transitions.¹³ Namely, it decreases the temperature of transition from paraelectric to ferroelectric phase in the bulk perovskites [compare Figs. 1(a) and 1(b)]. In some cases the hydrostatic pressure induces the transition to the relaxor state in the normal ferroelectrics (see, e.g., Ref. 23 and references therein). The lateral pressure (e.g., radial surface tension in cylindrical geometry) could induce the transition of a cubic unit cell into the nonpolar tetragonal one [see Fig. 1(c)]. Despite the lateral pressure conserves the inversion center, it leads to the short-range forces strengthening in the lateral direction (caused by the bond contraction) and their weakening in the z direction (caused by the bond elongation). As a result, the long-range correlations become more pronounced in the polar direction in comparison with the short-range forces. Allowing for the ferroelectricity cooperative nature,¹³ the tension stimulates the ferroelectric phase appearance at temperatures higher than the bulk Curie one.

The situation is more complex for the phase transitions in RS, since both high and low temperature Curie points shift to the higher temperatures and the region of the ferroelectric phase existence is widened.²⁴ Moreover, above the pressure about $4 \cdot 10^8$ Pa the upper Curie temperature is higher than the RS decomposition temperature 55°C . Our estimation of the radial pressure $\sigma \sim \mu/R$, related to the effective surface tension coefficient $\mu = 5, \dots, 50$ N/m, gives the value $10^8 - 10^9$ Pa for RS nanorods of radius 30 nm. This speaks in favor of the fact that the radial pressure caused by surface tension is responsible for the ferroelectricity enhancement in cylindrical nanorods.

II. FREE ENERGY OF NANOPARTICLE

Let us consider ferroelectric cylindrical nanoparticle with radius R , height h , and polarization $P_z(\rho, z)$ oriented along the z axes. Hereinafter $V = \pi R^2 h$ is the particle volume, the polarization distribution $P_z(\rho, z)$ is axisymmetric. The external electric field is $\mathbf{E} = (0, 0, E_0)$ [see Fig. 1(c)].

The Euler-Lagrange equation for the polarization can be obtained by the variation on polarization of the free energy functional $\Delta G = \Delta G_V + \Delta G_S$ consisted from the bulk part ΔG_V and the surface one ΔG_S (see, e.g., Ref. 15). The bulk part ΔG_V acquires the form

$$\Delta G_V = 2\pi \int_{-h/2}^{h/2} dz \int_0^R \rho d\rho \left(\frac{\alpha_R(T)}{2} P_Z^2(\rho, z) + \frac{\beta}{4} P_Z^4(\rho, z) + \frac{\gamma}{6} P_Z^6(\rho, z) + \frac{\delta}{2} [\nabla P_Z(\rho, z)]^2 - P_Z(\rho, z) \left[E_0 + \frac{E_Z^d(\rho, z)}{2} \right] \right). \quad (1)$$

Material coefficients $\delta > 0$ and $\gamma > 0$, while $\beta < 0$ for the first order phase transitions or $\beta > 0$ for the second order ones. The coefficient $\alpha_R(T)$ in Eq. (1) should be renormalized by the external stress (see, e.g., Refs. 21 and 25). In Appendix A we study the influence of the effective surface tension on a cylindrical particle and derived the expression for $\alpha_R(T)$

$$\alpha_R(T, R) = \alpha_T(T - T_C) + 2Q_{12} \frac{\mu}{R}. \quad (2)$$

Here parameters T_C and Q_{12} are, respectively, Curie temperature, and electrostriction coefficient, α_T is proportional to the inverse Curie constant regarded known for the bulk material. The parameter $\mu > 0$ is the effective surface tension coefficient between the nanoparticle and interface.^{26,10}

Equation (2) means that the surface tension in finite-size cylinders plays a role similar to an epitaxial strain in planar geometries (see, e.g., Ref. 14). The uniform radial pressure $p \sim \mu/R$ (compare with a compressive stress) compresses the cylindrical particle in the transverse direction and stretches it along the polar axis z . This strained state is favorable for the appearance of the spontaneous polarization, if the occurred spontaneous strain consists in the stretching along the polar axis and the lateral compression. This is true for the ferroelectrics with electrostriction coefficients $Q_{12} + Q_{13} < 0$ and $Q_{11} > 0$ (see Fig. 1).

Note that both signs of electrostriction coefficient Q_{12} and Q_{13} are possible for different materials, however $Q_{13} \equiv Q_{12} < 0$ for most of the perovskite ferroelectrics. In such a case the radial pressure coupled with polarization via electrostriction effect (similar to the epitaxial strain) can change the paraelectric-ferroelectric phase transition temperature T_C . Namely, we obtained from Eq. (2), that $T_C^* = T_C - 2Q_{12} \frac{\mu}{\alpha_T R}$ for the cylindrical particle with the polar axis that coincides with the cylinder one. Under the condition $Q_{12} < 0$, the temperature T_C^* is always higher than the one of the bulk material.

It should be noted that Huang *et al.*²¹ proposed the model in which the surface bond contraction induces a compressive stress $p \sim 1/R^2$ inside a spherical particle. However, the renormalization of coefficient $\alpha_R = \alpha + 2Q_{12}p$ for a cylindrical nanoparticle differs from the one $\alpha_R = \alpha + (Q_{11} + 2Q_{12})p$ obtained for a spherical particle.²¹ Both results are clear owing to the fact that stresses $\sigma_1 = \sigma_2 = -p$ and $\sigma_3 = 0$ for a cylinder (the pressure is not acting along the polar axis), whereas $\sigma_1 = \sigma_2 = \sigma_3 = -p$ for a sphere (the pressure is acting along the polar axis also). Note, that the condition $T_C^* > T_C$ is impossible for the spherical particles, where the sum $(Q_{11} + 2Q_{12})$ is positive. Also we did not take into account possible stress relaxation caused by dislocations. This approach used by many authors is valid for the small enough particle radius.²⁷

The depolarization electric field inside the finite cylindrical nanoparticle cannot be derived in the similar way as the field of the spherical one, because a finite cylinder is not a spheroid. The exact expression for depolarization field $\mathbf{E}^d(\rho, z)$ inside the cylindrical nanoparticle covered with screening charges is derived in Appendix B [see Eq. (B6)]. Hereinafter we use its Pade approximation

$$\begin{cases} E_Z^d(\rho, z) \approx \eta(R, h) \cdot [\langle P_Z \rangle - P_Z(\rho, z)], \\ \eta(R, h) = \frac{4\pi}{1 + (h/2R)^2}. \end{cases} \quad (3)$$

The angular brackets are the spatial averaging on the particle volume V , e.g.,

$$\langle P_Z \rangle \equiv \frac{2\pi}{V} \int_{-h/2}^{h/2} dz \int_0^R \rho d\rho P_Z(\rho, z).$$

The function $\eta \sim (2R/h)^2 \ll 1$ for the prolate cylinder with $R \ll h$,¹⁷ whereas $\eta \rightarrow 4\pi$ for the oblate cylinder with $R \gg h$.¹⁸ The depolarization field cross sections on the nanoparticle z and x axes are depicted in Fig. 2.

It should be noted that the depolarization field is absent outside the particles in the framework of our model. Therefore the interaction of such nanoparticles is practically absent due to the screening. Their composite can be considered as the assembly of independent particles.

The surface part of the polarization-dependent free energy ΔG_S is supposedly proportional to the square of polarization on the particle surface S , namely, $\Delta G_S = \frac{\delta}{2} \int_S \frac{ds}{\lambda} P_S^2$ (λ is the extrapolation length^{6,16}). A cylindrical nanoparticle has upper and bottom surfaces $z = h/2$, $z = -h/2$ and a sidewall $\rho = R$, so its surface energy ΔG_S acquires the form

$$\Delta G_S = \delta \left\{ \int_0^R \frac{2\pi\rho}{\lambda_b} d\rho \left[P_Z^2\left(\rho, z = \frac{h}{2}\right) + P_Z^2\left(\rho, z = -\frac{h}{2}\right) \right] + \int_{-h/2}^{h/2} \frac{2\pi R dz}{\lambda_s} P_Z^2(\rho = R, z) \right\}. \quad (4)$$

We introduced longitudinal and lateral extrapolation lengths $\lambda_b \neq \lambda_s$ in Eq. (4). Hereinafter we regard these extrapolation lengths positive.

Variation of the free energy expressions (1)–(4) yields the following Euler-Lagrange equations with the boundary conditions on the cylinder faces $z = \pm h/2$, and the sidewall surface $\rho = R$ (see, e.g., Ref. 6 and 19):

$$\left\{ \begin{array}{l} \alpha_R P_Z(\rho, z) + \beta P_Z^3(\rho, z) + \gamma P_Z^5(\rho, z) - \delta \left(\frac{\partial^2 P_Z(\rho, z)}{\partial z^2} + \frac{1}{\rho} \frac{\partial}{\partial \rho} \rho \frac{\partial}{\partial \rho} P_Z(\rho, z) \right) = E_0 + E_Z^d(\rho, z), \\ \left(P_Z + \lambda_b \frac{dP_Z}{dz} \right) \Big|_{z=h/2} = 0, \quad \left(P_Z - \lambda_b \frac{dP_Z}{dz} \right) \Big|_{z=-h/2} = 0, \quad \left(P_Z + \lambda_s \frac{dP_Z}{d\rho} \right) \Big|_{\rho=R} = 0, \end{array} \right. \quad (5)$$

In Appendix C we found the approximate solution of the nonlinear Eq. (5) by using the direct variational method as proposed earlier.¹⁹ The approach consists of the following:

(i) First we find the solution of the linearized Eq. (5) with respect to the boundary conditions. This exact analytical solution $P_Z(\rho, z)$ corresponds to the paraelectric phase of the system, where the nonlinearity can be neglected in the weak external field E_0 . The average paraelectric susceptibility $\langle \epsilon_{ZZ} \rangle = \frac{d\langle P_Z(\rho, z) \rangle}{dE_0} \Big|_{E_0=0}$ diverges in the point where the paraelectric phase loses its stability. The point coincides with the paraelectric-ferroelectric transition for the second order ferroelectrics. In such a case the exact expression for the transition temperature $T_{CN}(R, h)$ could be found directly from the condition $\langle \epsilon_{ZZ}^{-1}(T_{CN}, R, h) \rangle = 0$.

(ii) For the considered system the paraelectric solution has the form of the quickly converging series of linearly independent functions [see Eq. (C8)]. In order to study the system behavior in ferroelectric phase, these functions were chosen as the trial ones. Their amplitudes P_n are variational parameters. The trial series was substituted into the free energy $\Delta G = \Delta G_V + \Delta G_S$. After the integration over the particle volume we obtained the renormalized free energy in the form of polynomial series on P_n with coefficients depending on temperature T and the particle sizes R, h [see Eq. (C9)]. The variation amplitudes P_n can be determined from the algebraic equations obtained after the minimization of the renormalized free energy. When the dependence of polarization on temperature, particle sizes, and external field is calculated, other dielectric, pyroelectric, and piezoelectric properties can be determined from it in a conventional way.¹³

(iii) The direct variational method based on the exact paraelectric solution has the high accuracy even in the case of one-parametric trial functions.¹⁹ In the case of trial series the procedure has been easily realized numerically for the converging series. However, to our mind the main advantage of the method is the possibility to obtain the approximate analytical expressions for the transition temperature and renormalized coefficients size dependences.

Note, that Yadlovker and Berger¹ observed ferroelectric domains with walls oriented along the rod polar axis in a nanoparticle of RS. Keeping in mind that the domain wall energy are represented by the correlation term $\frac{\delta}{2} [\nabla P_Z(\rho, z)]^2$ in Eq. (1) for the continuous media approximation, polydomain states could be studied with the help of the free energy (1)–(4). However, for these states' adequate descriptions one should use the exact expression (B6) for the depolarization field and calculate the polarization distribution $P_Z(\rho, z) = \sum_{m=0}^{\infty} \sum_{n=1}^{\infty} P_{mn} \cos\left(\frac{2\pi m}{h} z\right) J_0\left(k_n \frac{\rho}{R}\right)$ in accordance with Eqs. (B7), (B6), and (5) self-consistently. The contour lines of depolarization field isopotential lines and spontane-

ous polarization spatial distribution for a single- and poly-domain states of the nanorod with $R=2h$ are depicted in Fig. 3.

III. PHASE DIAGRAM

In Appendix C we derived the interpolation for the paraelectric-ferroelectric transition temperature $T_{CN}(R, h)$ valid for the nanodisks, nanorods, and nanowires

$$T_{CN}(R, h) \approx T_C \left(1 - \frac{2\mu Q_{12}}{\alpha_T T_C R} - \frac{k_1^2 \delta}{\alpha_T T_C R^2} - \frac{2\eta(R, h)}{\alpha_T T_C (1 + \lambda_b \xi) \xi h} \right), \quad (6)$$

where $\xi(R, h) = \sqrt{\frac{1}{\delta} \left(\frac{k_1^2 \delta}{R^2} + \eta(R, h) \right)}$, $k_1 \approx 2.405$.

The first term in Eq. (6) is the bulk transition temperature, the second term is related to the coupling of surface tension with polarization via electrostriction effect, the third one corresponds to the correlation effects, and the fourth represents the depolarization field contribution. The depolarization field is small enough at $h \gg R$. The correlation and depolarization terms are always negative and thus only decrease the transition temperature, whereas the second electrostriction term $\frac{2\mu Q_{12}}{\alpha_T T_C R}$ in Eq. (6) could be positive or negative depending on the Q_{12} sign. Note, that both signs of Q_{12} are possible for different ferroelectrics, however $Q_{12} < 0$ and $Q_{11} + 2Q_{12} > 0$ for most of the perovskite ferroelectrics. Below we demonstrate that increasing of transition temperature and thus ferroelectric properties enhancement and conservation is possible when $\frac{2\mu Q_{12}}{\alpha_T T_C R} < 0$ and depolarization field is small enough. The latter is impossible for the spherical particles with positive renormalization $(Q_{11} + 2Q_{12})\mu > 0$.²¹

Let us make some estimations of the second and third terms in Eq. (6) for perovskites BaTiO₃ and PbTiO₃. Using parameters $Q_{12} = -0.043 \text{ m}^4/\text{C}^2$, $T_C = 400 \text{ K}$ (BaTiO₃) and $Q_{12} = -0.046 \text{ m}^4/\text{C}^2$, $T_C = 666 \text{ K}$ (PbZr_{0.5}Ti_{0.5}O₃) and $\mu = 5 - 50 \text{ N/m}$ (see, e.g., Ref. 10), $\delta = 10^{-19} \text{ m}^2$, we obtained that

$$\left| \frac{2\mu Q_{12}}{\alpha_T T_C} \right| \approx 2 - 17 \text{ nm}, \quad \sqrt{\frac{\delta k_1^2}{\alpha_T T_C}} \approx 5 \text{ nm} \quad \text{for BaTiO}_3$$

and

$$\left| \frac{2\mu Q_{12}}{\alpha_T T_C} \right| \approx 3 - 26 \text{ nm}, \quad \sqrt{\frac{\delta k_1^2}{\alpha_T T_C}} \approx 5 \text{ nm}$$

for PbZr_{0.5}Ti_{0.5}O₃,

respectively. So both terms are comparable with unity at nanoparticle radius $\sim 2 - 25 \text{ nm}$.

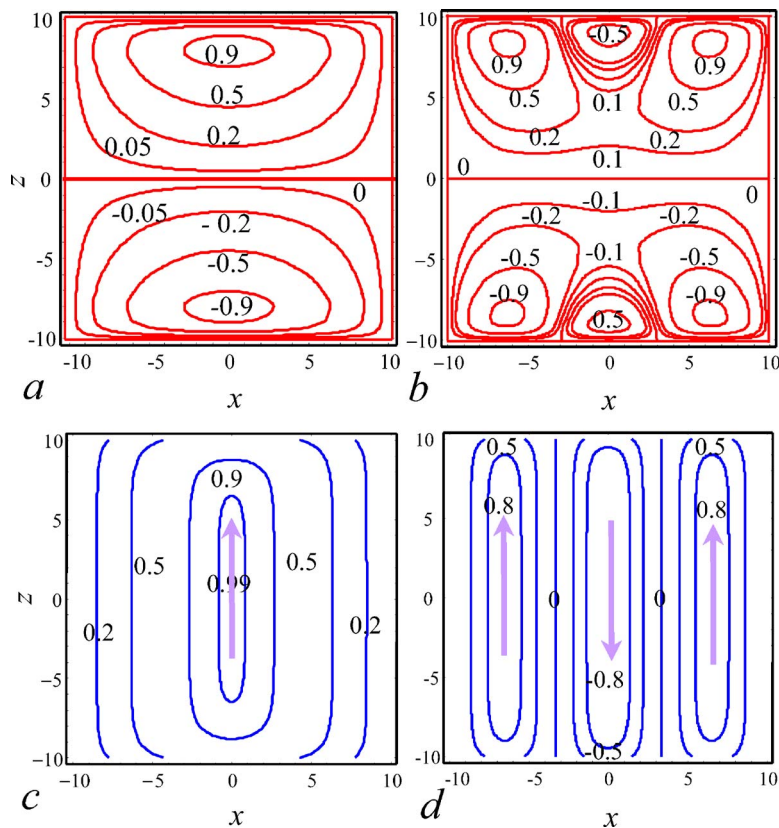


FIG. 3. (Color online) Depolarization field isopotential lines (a), (b) and contour lines of spontaneous polarization spatial distribution (c), (d) for a single- (a), (c) and poly-domain states (b), (d) of the nanorod with $h=2R$. Numbers near curves correspond to the values of polarization and potential normalized on their maximal values.

For a bulk sample $R \rightarrow \infty$ and $h \rightarrow \infty$, so one obtains that $T_{CN}(R, h) \rightarrow T_C$ as it should be expected. For a nanodisk $R \gg h$, so values $\eta \rightarrow 4\pi$ and $\xi \rightarrow \sqrt{4\pi\delta}$, thus the renormalized transition temperature acquires the form similar to the one derived in Ref. 20. For a nanowire $h \rightarrow \infty$, so the depolarization field vanishes ($\eta \rightarrow 0$), thus

$$T_{CN}(R, h) \approx T_C - \frac{2\mu Q_{12}}{\alpha_T R} - \frac{k_1^2 \delta}{\alpha_T R^2}.$$

Taking into account that the gradient coefficient $\sqrt{\delta} \sim 0.3, \dots, 0.5$ nm, i.e., it is of a lattice constant order, we

introduced the parameters and dimensionless variables that correspond to the lattice constants units

$$R_\mu = \frac{2\mu Q_{12}}{\alpha_T T_C \sqrt{\delta}}, \quad R_S = \sqrt{\frac{k_1^2}{\alpha_T T_C}}, \quad r = \frac{R}{\sqrt{\delta}}, \quad l = \frac{h}{\sqrt{\delta}}, \quad (7)$$

$$\Lambda_b = \frac{\lambda_b}{\sqrt{\delta}}, \quad \Lambda_S = \frac{\lambda_S}{\sqrt{\delta}}.$$

In these variables

$$\begin{cases} T_{CN}(r, l) \approx T_C \left(1 - \frac{R_\mu}{r} - \frac{R_S^2}{r^2} - \frac{2\eta(r, l)}{\alpha_T T_C [1 + \Lambda_b \zeta(r, l)] \zeta(r, l) l} \right), \\ \zeta(r, l) = \sqrt{\left(\frac{k_1^2}{r^2} + \eta(r, l) \right)}, \quad k_1 \approx 2.405. \end{cases} \quad (8)$$

Let us underline, that R_μ sign is determined by the one of electrostriction coefficient Q_{12} (surface tension coefficient μ is regarded positive). So, the parameter R_μ is negative for most of perovskites with $Q_{12} < 0$. In accordance with our estimations [see comments to Eq. (6)] we obtained that $R_S \sim 10, \dots, 20$ and $|R_\mu| \sim 8, \dots, 80$ depending on the mate-

rial parameters and surface tension coefficient value, respectively.

In order to study the surface tension influence on the transition temperature, one has to vary the term $\frac{R_\mu}{r} \sim \frac{\mu Q_{12}}{R}$ experimentally. The surface tension coefficient μ is determined by the interaction of the material with the outer media. So, one

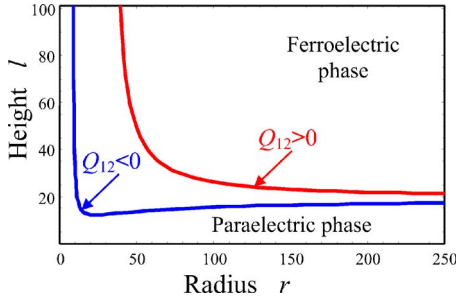


FIG. 4. (Color online) Cylindrical nanoparticles phase diagram. Parameters: $\alpha_T T_C = 3 \cdot 10^{-2}$, $\Lambda_S \leq 1$ and $\Lambda_b = 5$, $R_\mu = \pm 25$, $R_S = 17$. In Figs. 2–4 material parameters correspond to $\text{PbZr}_{0.5}\text{Ti}_{0.5}\text{O}_3$. Note, that the dimensionless size $r \sim 1$ or ($l \sim 1$) corresponds to the one lattice constant.

could tune the surface tension coefficient μ by changing the nanoparticle surrounding, e.g., to grow nanorods in cylindrical porous made of different oxides.

However, probably the simplest way to tune the dimensionless ratio R_μ/r is to vary the cylinder radius, e.g., by fitting the average porous sizes, sieves, etc. The quantitative comparison of the measured dependence $T_{CN}(r)$ with the one calculated from Eq. (8) would be extremely desirable in order to verify our theoretical results. One could say that the surface tension influence is key to the ferroelectricity enhancement in confined nanorods, if it is appeared that the dependence $T_{CN}(r)$ has the form

$$T_{CN}(r) \approx T_C \left(1 - \frac{R_\mu}{r} - \frac{R_S^2}{r^2} \right)$$

for a long nanorod or nanowire ($l \gg r$), where R_μ is negative, the fitting parameters R_μ and R_S values are reasonable [see Eq. (7) for definitions].

In Figs. 4–6 we present phase diagrams calculations based on the Eq. (7).

The critical sizes can be found from the equation $T_{CN}(r, l) = 0$, i.e., dependence $l_{cr}(r)$ determines the boundary between the paraelectric and ferroelectric phase (see and bold solid curves in the Fig. 4). It is clear that the region of ferroelectric phase existence appreciably broadens at $R_\mu < 0$ in comparison with the one at $R_\mu > 0$. In fact, at chosen material parameters ferroelectric phase is absent in the nanocylinders with height $l \leq 22$ ($R_\mu = +25$) or $l \leq 12$ ($R_\mu = -25$) and arbitrary radius. On the other hand ferroelectric phase is absent in the nanorods with radius $r \leq 40$ ($R_\mu = +25$) or $r \leq 8$ ($R_\mu = -25$) and arbitrary height. Depolarization field and lateral correlation effects cause the aforementioned size-induced transition to paraelectric phase.

The size effect on the phase diagram for the case when the shape of nanoparticle is fixed ($l/2r = \text{const}$), but its radius r or length l varies is represented in Figs. 5(a) and 5(b), respectively. It is clear from the figures that transition temperature values are different for nanowires ($l/2r \geq 100$), nanorods ($l/2r \geq 10$), nanobars $l/2r \approx 1$, and nanodisks $l/2r \leq 0.1$. The transition temperature tends to the bulk value T_C at $r \rightarrow \infty$ and $l \rightarrow \infty$ for any shape, as it should be expected for the bulk ferroelectric material.

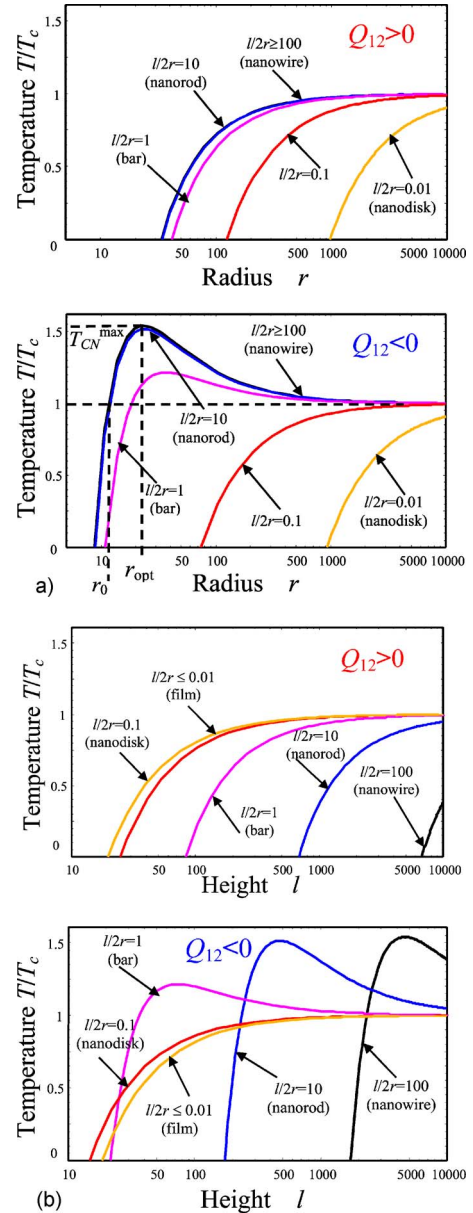


FIG. 5. (Color online) (a) Transition temperature size dependence for different ratios $l/2r = 100, 10, 1, 0.1$, and 0.01 . Other parameters: $\alpha_T T_C = 2.8 \cdot 10^{-2}$, $\Lambda_S \leq 1$, $R_\mu = \pm 25$, $R_S = 17$, and $\Lambda_b = 5$. (b) Transition temperature size dependence for different ratios $l/2r = 100, 10, 1, 0.1$, and 0.01 . Other parameters: $\alpha_T T_C = 2.8 \cdot 10^{-2}$, $\Lambda_S \leq 1$, $R_\mu = \pm 25$, $R_S = 17$, and $\Lambda_b = 5$.

As it follows from Figs. 5(a), the transition temperature $T_{CN}(r)$ is the highest for the nanowire, where depolarization field is absent, and only the correlation effect and surface tension determine the size dependence of paraelectric-ferroelectric transition temperature. The results are approximately the same for the nanorods with $l/2r \geq 10$. $T_{CN}(r)$ is the lowest for the nanodisks with $l/2r = 0.01$ because of the maximal depolarization factor $\eta \approx 4\pi$. The critical radius is minimal for nanowires and nanorods and increases with $l/2r$ increase both for $R_\mu < 0$ and $R_\mu > 0$. It is clear from Fig. 5(a) that the transition temperature $T_{CN}(r)$ between the paraelectric and ferroelectric phase increases monotonically with

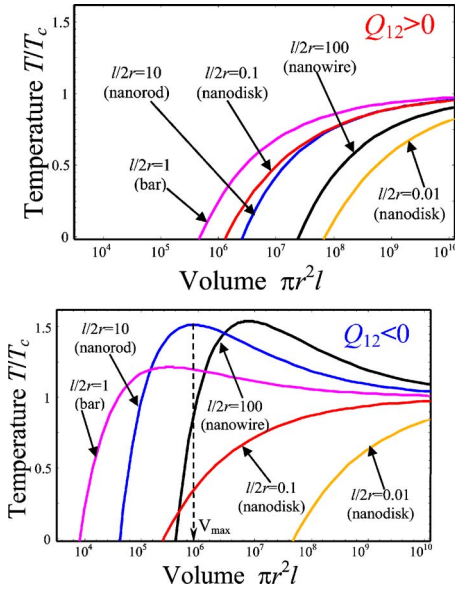


FIG. 6. (Color online) Transition temperature versus particle volume for different ratios $l/2r=100, 10, 1, 0.1$, and 0.01 . Other parameters: $\alpha_T T_C = 2.8 \cdot 10^{-2}$, $\Lambda_S \leq 1$, $R_\mu = \pm 25$, and $R_S = 17$, $\Lambda_b = 5$. Note, that the dimensionless volume of 10^{10} is about 10^{10} unit cells, that corresponds to the $0.64 \mu\text{m}^3$ and to the linear size of 860 nm .

nanoparticle radius increasing only for $R_\mu > 0$.

For $R_\mu < 0$ nanowires, nanorods, and nanobars reveal the increase of transition temperature $T_{CN}(r)/T_C > 1$ in the region $r \geq r_0(l)$. No enhancement was obtained for nanodisks [$T_{CN}(r)/T_C$ is always smaller than unity].

In accordance with our model, the main reason of transition temperature decrease in nanodisks is the strong depolarization field (in the absence of domain structure they have the highest depolarization factor 4π at $r \gg l$). Note that the lateral correlation effects and effective surface pressure can be neglected for nanodisks with $r \gg |R_\mu|$ and $r \gg R_S$ as proportional to R_S^2/r and R_μ/r , correspondingly. The depolarization field decreases in the presence of domains, but in any case it can only decrease the transition temperature less or more in comparison with the bulk one.

Prolate nanorods and nanowires possess a much smaller depolarization field [their depolarization factor is proportional to $(r/l)^2$]. Note that the existence of a polydomain structure leads to the additional decrease of a depolarization field [compare, e.g., Figs. 3(a) and 3(b)]. Thus, under the absence of correlation effects (proportional to R_S^2/r^2) and surface pressure influence (proportional to R_μ/r) the nanorod transition temperature is almost equal to the bulk one. The correlation effect always leads to the transition temperature decrease under the radius decrease. The surface tension increases the transition temperature via the negative electrostriction effect $Q_{12} < 0$. Under the favorable conditions $R_\mu \sim Q_{12}\mu < 0$, $|R_\mu| \approx R_S$ and $r \approx R_S$ the competition between these two lateral contributions leads to the increase of the transition temperature up to

$$T_{CN}^{\max}(r_{\text{opt}}) = T_C \left(1 + \frac{R_\mu^2}{4R_S^2} \right) \quad \text{at radius } r_{\text{opt}} = \frac{2R_S^2}{R_\mu}$$

($T_{CN}^{\max}/T_C \approx 1.5$, $r_{\text{opt}} \approx 20$). The increase of transition temperature $T_{CN}(r)/T_C > 1$ exists in the region $r \geq r_{\text{opt}}/2$.

Figure 5(b) demonstrates that the transition temperature $T_{CN}(l)$ decreases monotonically with the ratio $l/2r$ increase only for $R_\mu > 0$, namely, the nanodisks have the maximal transition temperature, whereas nanowires have the minimal one. For $R_\mu < 0$ nanowires and nanorods reveal the increase of transition temperature up to $T_{CN}^{\max} \approx 1.5T_C$ at some l_{opt} values. Both for $R_\mu < 0$ and $R_\mu > 0$ the nanodisks have the minimal critical length $l_{\text{cr}} \sim 20$, whereas nanowires have the maximal critical length $l_{\text{cr}} \sim 2000-5000$. These results become clear taking into account that at fixed height l the phase transition in the nanodisk ($2r \gg l$) is influenced minimally by the lateral correlation effects [i.e., the second and third terms proportional to $1/r$ and $1/r^2$ in Eq. (6) are small in comparison with the ones for the nanorod ($2r \ll l$)].

It seems natural that the lateral correlation effect on the size-driven phase transition reveals itself at fixed height, whereas the depolarization field influence on critical sizes and transition temperature is more pronounced at fixed radius [compare curves order for different ratio $l/2r$ in Figs. 5(b) and 5(a)].

Finally, let us answer the important question: “What nanoparticle shape possesses the minimal critical volume and allows ferroelectricity conservation at higher temperatures?” For this purpose we have to consider the case when the shape of the nanoparticle is fixed ($l/2r = \text{const}$), but its volume $\pi r^2 l$ increases. The results are represented in Figs. 6. It follows from the figures that the nanobar ($l/2r=1$, depolarization factor $\eta \approx 2\pi$) has the smallest critical volume both at $R_\mu > 0$ and at $R_\mu < 0$. Its ferroelectric-paraelectric transition temperature is high enough up to the values higher than T_C . Moreover, since $R_\mu \sim Q_{12}\mu < 0$ this nanoparticle shape is preferable in comparison with a spherical one, because a sphere has positive parameter $R_\mu \sim (Q_{11} + 2Q_{12})\mu$ and only slightly smaller depolarization factor $\eta = 4\pi/3$.²⁰ The nanorods with the shape $10 < l/2r \leq 100$ reveal the highest transition temperature and thus the best ferroelectric properties in the region of volumes $V > V_{\text{max}}$ at $R_\mu < 0$.

Both for $R_\mu > 0$ and $R_\mu < 0$, the dependence of transition temperature on the nanoparticle volume for different shapes $l/2r$ is nonmonotonic with respect to the ratio $l/2r$ in contrast to the monotonic radius dependencies [compare Figs. 6 with the Figs. 5(a)]. Let us underline that under the condition $R_\mu < 0$ nanobars and prolate nanorods ($1 \leq l/2r \leq 10$) possess enhanced polar properties at $r \sim (10-200)$ unit cells, namely, they have higher spontaneous polarization and transition temperature in comparison with a bulk sample, and the nanobar reveals the minimal critical volume.

IV. DISCUSSION

Why is the transition temperature depressed in nanodisks but enhanced in nanorods? Assuming that the surface tension in finite-size cylinders plays a similar role as an epitaxial

strain in thin films, we propose the following physical explanation of the phenomena:

(i) The lateral correlation effects and radial pressure originating from the effective surface tension can be neglected for nanodisks since their contributions are proportional to $1/R^2$ and $1/R$, correspondingly. However, the strong depolarization field is the main reason of transition temperature decrease in nanodisks under their height h decrease (in the absence of the domain structure they have the highest depolarization factor 4π at $R \gg h$). The depolarization field decreases in the presence of domains, but in any case it can only decrease the transition temperature less or more. Thus, the nanodisk transition temperature is smaller than the bulk one; it reveals no enhancement and tends to the zero near the critical height.

(ii) Prolate nanorods and nanowires possess much smaller depolarization fields [their depolarization factors are proportional to $(R/h)^2$ and tends to zero for an infinite cylinder]. Note that the existence of polydomain structure leads to the additional decrease of the depolarization field and thus improves the estimation. Therefore the field could be neglected at all in the further qualitative explanation. Thus, under the absence of correlation effects and surface pressure influence the nanorod transition temperature is almost equal to the bulk one. The correlation effect $\sim \delta/R^2$ reflects the ferroelectricity cooperative nature¹³ and always causes the decreases of the transition temperature with radius decreasing. The surface pressure $p \sim \mu/R$ (similar to the epitaxial strains) can increase the transition temperature via electrostriction effect (i.e., when the effective surface pressure leads to the decrease of the inverse dielectric susceptibility due to the negative electrostriction coefficient $Q_{12} < 0$). Under the favorable conditions the competition between these two lateral contributions leads to the increase of the transition temperature (see Figs. 5 and 6). In accordance with our estimations the transition temperature maximum

$$T_{CN}^{\max}(R_{\text{opt}}) \approx T_C + 0.17 \frac{\mu^2 Q_{12}^2}{\alpha_T \delta}$$

appeared at radius $R_{\text{opt}} \approx -\frac{4\delta}{\mu Q_{12}}$ that corresponds to the lateral size of 10–100 lattice constants. The noticeable increase of the transition temperature exists in the region of 5–500 lattice constants.

(iii) The influence of the depolarization field could be studied experimentally by varying the nanorod height h . However, the additional investigation of the domain structure behavior at different heights is desirable. The dependence $T_{CN}(h)$ with maximum at $h \sim 10^2$ – 10^3 unit cells under the reasonable values of fitting parameters would speak in favor of our model.

(iv) How can the surface tension influence on the ferroelectricity conservation in confined nanorods be verified experimentally? The compressive lateral stress is determined by the ratio μ/R (Q_{12} is regarded known). In order to study the surface tension influence one has to vary this term experimentally. The surface tension coefficient μ is determined by the interaction of the material with the outer media. So, one could tune the surface tension coefficient μ by changing

the nanoparticle surrounding, e.g., to grow nanorods in cylindrical porous made of different oxides. Also defects and surface-active substances tend to decrease the surface energy, thus one can try to anneal the nanocomposite at different temperatures. However, probably the simplest way to tune the dimensionless ratio $\mu Q_{12}/R$ is to vary the cylinder radius R , e.g., by fitting the average porous sizes, sieves, etc. The quantitative comparison of the measured dependence $T_{CN}(R)$ with the one calculated from Eqs. (7) and (8) would be extremely desirable in order to verify our model. If it appears that Eq. (8) is valid at the reasonable values of fitting parameters, one could say that the surface tension influence is key to the ferroelectricity enhancement in confined nanorods.

The ferroelectricity enhancement has the microscopic explanation. For the ferroelectrics of displacement type the transition temperature from the paraelectric to ferroelectric phase is determined by the difference between long-range and short-range force constants (see, e.g., chap. 4 in Ref. 28 and chap. 2 in Ref. 13). The transition temperature decreases when the short-range forces are strengthened. The radial pressure shifts ions from their equilibrium positions in cubic lattice [compare Figs. 1(a) and 1(c)]. Therefore the potential energy of ions changes since the short-range interactions are strongly sensitive to the interion distances. Namely, these forces are weakened along the axis preferred by the radial pressure and strengthened in the perpendicular directions. At the same time the long-range forces determining intercell interactions remain practically the same. Therefore the ferroelectric instability is reinforced along the preferred axis and the transition temperature increases.

Finally, let us qualitatively compare our results with the ones obtained earlier^{1,2,11} (see Table I). The applicability of our model to the description of phase transition between cubic paraelectric and tetragonal ferroelectric phases in BT and PZT is for certain. However, RS is known to be improper ferroelastic-ferroelectric, therefore our consideration can be applied to experiments of Yadlovker and Berger¹ only in the temperature range where RS ferroelectric properties can be described by the phenomenological expansion (1) over polarization powers. Moreover, we neglected the piezoelectric effect with respect to the shear stress in the paraelectric phase of RS since the effective surface tension creates no tangential stresses.

Despite the aforementioned warning, obtained results explain ferroelectricity enhancement in the Rochelle salt nanorods¹ of radius ~ 30 nm, piezoelectric properties conservation in lead-zirconate-titanate nanorods¹¹ of radius ~ 5 – 10 nm and are in a good agreement with the first principles calculations in barium titanate nanowires.² The predicted effects could be very useful for elaboration of modern nanocomposites with perfect polar properties.

ACKNOWLEDGMENT

Research was partially supported by the Science and Technology Center in Ukraine, Project No. 3898.

APPENDIX A

The free energy expansion on polarization $\mathbf{P}=(0,0,P_3)$ and stress σ_i powers has the following form:^{21,14}

TABLE I. Comparison with experiment.

Material	Experiment ^a or <i>ab initio</i> calculations ^b			Proposed model						
	h (nm)	R_{cr} (nm)	T_{cr} (K)	Calculated critical parameters	Material constants used in calculations					
				R_{cr} (nm)	R_{opt} (nm)	T_{CN}^{max} (K)	T_C (K)	Q_{12} (m ⁴ /C ²)	δ (10 ⁻¹⁹ m ²)	μ (N/m)
PZT 50/50	$\gg R$	5-10	300	1.1-5.3 at 300 K	2-23	704 melt	665.7	-0.046	1	50-5
BT	$\gg R$	1.2	0	1.1-3.8 at 0 K	2-24	414 melt	400	-0.043	1	50-5
RS	500	≤ 30	328	11-24 at 300 K	33	300 melt	297	$Q_{12}=1.56^c$ $Q_{13}=-2.19^c$	10	5-0.5

^aReferences 1 and 11.^bReference 2.^cReference 29.

$$\begin{aligned}
F = & a_1 P_3^2 + a_{11} P_3^4 + a_{111} P_3^6 - Q_{11} \sigma_3 P_3^2 - Q_{12} (\sigma_1 + \sigma_2) P_3^2 \\
& - \frac{1}{2} s_{11} (\sigma_1^2 + \sigma_2^2 + \sigma_3^2) - s_{12} (\sigma_1 \sigma_2 + \sigma_1 \sigma_3 + \sigma_3 \sigma_2) \\
& - \frac{1}{2} s_{44} (\sigma_4^2 + \sigma_5^2 + \sigma_6^2). \tag{A1}
\end{aligned}$$

Hereinafter we use Voigt notation σ_i or matrix notation σ_{nm} ($xx=1, yy=2, zz=3, zy=4, zx=5, xy=6$) when it necessary.

First, let us calculate the σ_i components caused by the uniform lateral pressure related to the effective surface tension $p = \mu/R$.^{26,10} This Lamé's problem is discussed in details elsewhere.³⁰ It is easy to obtain that generalized pressure is directed along the cylinder normal, i.e., $\mathbf{p} \uparrow \mathbf{n}$. The conditions of mechanical equilibrium $n_i \sigma_{ij} = -p_j$ on the surface of the cylindrical solid body have the following form in the cylindrical coordinates (ρ, φ, z) :

$$\sigma_{\rho\rho}|_{\rho=R} = -p, \quad \sigma_{\rho\varphi}|_{\rho=R} = 0, \quad \sigma_{\rho z}|_{\rho=R} = 0, \quad \sigma_{zz}|_{z=\pm h/2} = 0, \tag{A2}$$

$$\sigma_{z\rho}|_{z=\pm h/2} = 0, \quad \sigma_{z\varphi}|_{z=\pm h/2} = 0.$$

The conditions of mechanical equilibrium $\partial\sigma_{ij}/\partial x_i = 0$ in the bulk of solid body are the following:

$$\begin{cases}
\frac{\partial\sigma_{zz}}{\partial z} + \frac{\partial\sigma_{z\rho}}{\partial\rho} + \frac{\sigma_{z\rho}}{\rho} + \frac{1}{\rho} \frac{\partial\sigma_{z\varphi}}{\partial\varphi} = 0, \\
\frac{\partial\sigma_{\rho\rho}}{\partial\rho} + \frac{\sigma_{\rho\rho} - \sigma_{\varphi\varphi}}{\rho} + \frac{1}{\rho} \frac{\partial\sigma_{\rho\varphi}}{\partial\varphi} + \frac{\partial\sigma_{z\rho}}{\partial z} = 0, \\
\frac{1}{\rho} \frac{\partial\sigma_{\varphi\varphi}}{\partial\varphi} + \frac{\partial\sigma_{z\varphi}}{\partial z} + \frac{\partial\sigma_{\rho\varphi}}{\partial\rho} + 2 \frac{\sigma_{\rho\varphi}}{\rho} = 0.
\end{cases} \tag{A3}$$

It is seen that boundary and equilibrium conditions (A2) and (A3) can be fulfilled with

$$\sigma_{\rho\rho} = \sigma_{\varphi\varphi} = -p, \quad \sigma_{\rho\varphi} = 0, \quad \sigma_{\rho z} = 0, \quad \sigma_{zz} = 0, \quad \sigma_{z\varphi} = 0. \tag{A4}$$

The tensor components in Cartesian coordinates can be found from relations

$$\begin{pmatrix} \sigma_{xx} & \sigma_{xy} & \sigma_{xz} \\ \sigma_{yx} & \sigma_{yy} & \sigma_{yz} \\ \sigma_{zx} & \sigma_{zy} & \sigma_{zz} \end{pmatrix} = \begin{pmatrix} \cos(\varphi) & -\sin(\varphi) & 0 \\ \sin(\varphi) & \cos(\varphi) & 0 \\ 0 & 0 & 1 \end{pmatrix} \cdot \begin{pmatrix} \sigma_{\rho\rho} & \sigma_{\rho\varphi} & \sigma_{\rho z} \\ \sigma_{\varphi\rho} & \sigma_{\varphi\varphi} & \sigma_{\varphi z} \\ \sigma_{z\rho} & \sigma_{z\varphi} & \sigma_{zz} \end{pmatrix} \cdot \begin{pmatrix} \cos(\varphi) & \sin(\varphi) & 0 \\ -\sin(\varphi) & \cos(\varphi) & 0 \\ 0 & 0 & 1 \end{pmatrix}. \tag{A5}$$

Allowing for Eq. (A4), expression (A5) leads to

$$\sigma_{xx} = \cos(\varphi)^2 \sigma_{\rho\rho} + \sin(\varphi)^2 \sigma_{\varphi\varphi} = -p,$$

$$\sigma_{yy} = \sin(\varphi)^2 \sigma_{\rho\rho} + \cos(\varphi)^2 \sigma_{\varphi\varphi} = -p,$$

$$\sigma_{xy} = \cos(\varphi)\sin(\varphi)(\sigma_{\rho\rho} - \sigma_{\varphi\varphi}) = 0,$$

$$\sigma_{xz} = \sigma_{yz} = \sigma_{zz} = 0. \tag{A6}$$

In Voigt notation this gives

$$\sigma_1 = \sigma_2 = -\frac{\mu}{R}, \quad \sigma_3 = \sigma_4 = \sigma_5 = \sigma_6 = 0. \tag{A7}$$

The ansatz of solutions (A7) into the free energy (A1) gives the expression

$$F = \left(a_1 + 2Q_{12} \frac{\mu}{R} \right) P_3^2 + a_{11} P_3^4 + a_{111} P_3^6 - (s_{11} + s_{12}) \frac{\mu^2}{R^2}. \quad (\text{A8})$$

The minimization of free energy (A8) on the polarization components $\partial F / \partial P_3 = E_0$ gives the equation of state.

Note, that the renormalization of coefficient $a_1^* = (a_1 + 2Q_{12}p)$ for a cylindrical nanoparticle differs from the one $a_1^* = [a_1 + (Q_{11} + 2Q_{12})P]$ obtained for a spherical nanoparticle recently.²¹ Both results are clear owing to the fact that $\sigma_1 = \sigma_2 = -p$ and $\sigma_3 = 0$ for a cylinder, whereas $\sigma_1 = \sigma_2 = \sigma_3 = -p$ for a sphere. Also let us underline that we do not take into account possible stress relaxation caused by dislocations and disclinations. This approach used by many authors (see, e.g., Refs. 14, 21, and 30) is valid under the conditions discussed elsewhere.²⁷

Let us underline that the surface tension does not affect the quartic term, in contrast to the films. The reasons are the following:

(i) The epitaxial thin film is under so-called ‘‘mixed’’ mechanical boundary conditions. Namely, the normal components of the stress tensor are zero on the upper surface of the film and on the film-substrate interface the displacement components are governed by the misfit between thin film and thick substrate. Since the conventional form of the free energy corresponds to the case of the stress tensor fixed components (free or compressed samples), ‘‘mixed’’ boundary conditions lead to the renormalization of the quartic terms in the free energy (this question is discussed in detail earlier¹⁴).

(ii) In the case of a cylindrical particle the mechanical boundary conditions corresponds to the first order ones, since the components of the stress tensor are fixed, namely, the lateral ones are determined by the surface tension, the longitudinal and shear ones are zero. Therefore the renormalization of the quartic terms in the free energy does not take place. It should be noted that Huang *et al.*²¹ also renormal-

ized only the quadratic term, but not the quartic one.

APPENDIX B

Let us consider the depolarization field distribution for the case of cylindrical particle with arbitrary polarization distribution in the ambient conditions. In the equilibrium the perfect screening can be achieved so that there will be no electric field outside the particle.

The field distribution can be obtained on the basis of the electrostatic Poisson’s equation for the electric potential φ

$$\Delta \varphi(\rho, z) = 4\pi \operatorname{div} \mathbf{P}(\rho, z). \quad (\text{B1})$$

Here $\mathbf{P}(\rho, z) = (0, 0, P_z)$ is the given z -component polarization distribution inside the particle, which has the cylindrical symmetry: $\Delta = \partial^2 / \partial z^2 + 1/\rho (\partial / \partial \rho) \rho (\partial / \partial \rho)$. The boundary conditions on the particle surface has the view

$$\varphi(\rho = R, z) = 0, \quad \varphi\left(\rho, z = -\frac{h}{2}\right) = 0, \quad \varphi\left(\rho, z = \frac{h}{2}\right) = U. \quad (\text{B2})$$

Here R and h is the cylinder radius and height, respectively, U is the applied voltage. At $U=0$ the boundary conditions (B2) corresponds to the short-circuit ones proposed by Kretschmer and Binder¹⁸ for a film.

The systems (B1) and (B2) can be solved by means of the separation of variables method. Since for the system of cylindrical symmetry eigenfunctions of Laplace operator Δ are the Bessel functions one can find the potential φ in the form of series

$$\varphi(\rho, z) = \sum_{n=1}^{\infty} C_n(z) J_0\left(k_n \frac{\rho}{R}\right). \quad (\text{B3})$$

Here $J_0(x)$ is the first kind Bessel function of zero order, k_n is the n -th root of this function [$J_0(k_n) = 0$], and functions $C_n(z)$ should satisfy the following boundary problem:

$$\begin{cases} \frac{d^2 C_n(z)}{dz^2} - \left(\frac{k_n}{R}\right)^2 C_n(z) = 4\pi \frac{2}{R^2 J_1(k_n)^2} \int_0^R \frac{\partial P_z(\rho, z)}{\partial z} J_0\left(k_n \frac{\rho}{R}\right) \rho d\rho \\ C_n\left(z = -\frac{h}{2}\right) = 0, \quad C_n\left(z = \frac{h}{2}\right) = \frac{2}{k_n J_1(k_n)} U \end{cases}. \quad (\text{B4})$$

In Eq. (B4) we used the Bessel functions orthogonality

$$\int_0^R J_0\left(k_n \frac{\rho}{R}\right) J_0\left(k_m \frac{\rho}{R}\right) \rho d\rho = \delta_{nm} \frac{[R^2 J_1(k_n)^2]}{2},$$

integral

$$\int_0^R J_0\left(k_n \frac{\rho}{R}\right) \rho d\rho = R^2 \frac{J_1(k_n)}{k_n}$$

and expansion

$$1 = \sum_{n=1}^{\infty} \frac{2}{[k_n J_1(k_n)]} J_0\left(k_n \frac{\rho}{R}\right) \quad \text{at } \rho < R.$$

In accordance with the general theory of the linear second order differential equations one can find the solution of Eq. (B4) in the form

$$C_n(z) = \sum_{m=1}^{\infty} g_{nm} \sin\left(\frac{2\pi m z}{h}\right) + A_n \exp\left(\frac{k_n z}{R}\right) + B_n \exp\left(-\frac{k_n z}{R}\right),$$

$$g_{mn} = -\frac{4\pi}{\left(\frac{2\pi m}{h}\right)^2 + \left(\frac{k_n}{R}\right)^2} \int_{-h/2}^{h/2} \frac{2dz}{h} \sin\left(\frac{2\pi m z}{h}\right) \times \int_0^R \frac{2\rho d\rho}{R^2 J_1(k_n)^2} J_0\left(k_n \frac{\rho}{R}\right) \frac{\partial P_z(\rho, z)}{\partial z},$$

$$A_n = \frac{2U}{k_n J_1(k_n)} \frac{\exp\left(-\frac{k_n h}{2R}\right)}{1 - \exp\left(-\frac{2k_n h}{R}\right)}, \quad (\text{B5})$$

$$B_n = -\frac{2U}{k_n J_1(k_n)} \frac{\exp\left(-\frac{3k_n h}{2R}\right)}{1 - \exp\left(-\frac{2k_n h}{R}\right)}.$$

Keeping in mind Eqs. (B3) and (B5), one obtains that depolarization field z component $E_Z^d = -\partial\varphi(\rho, z)/\partial z$ acquires the form after integrating over parts

$$E_Z^d(\rho, z) = \sum_{m=1}^{\infty} \sum_{n=1}^{\infty} E_{mn} \cos\left(\frac{2\pi m}{h} z\right) J_0\left(k_n \frac{\rho}{R}\right),$$

$$E_{mn} = -4\pi \frac{(2\pi m R)^2}{(2\pi m R)^2 + (k_n h)^2} P_{mn},$$

$$P_{mn} = \int_{-h/2}^{h/2} \frac{2d\tilde{z}}{h} \cos\left(\frac{2\pi m}{h} \tilde{z}\right) \int_0^R \frac{2\tilde{\rho} d\tilde{\rho}}{R^2 J_1(k_n)^2} J_0\left(k_n \frac{\tilde{\rho}}{R}\right) P_Z(\tilde{\rho}, \tilde{z}). \quad (\text{B6})$$

Note, that coefficients P_{mn} coincide with the ones in polarization expansion

$$P_Z(\rho, z) = \sum_{m=0}^{\infty} \sum_{n=1}^{\infty} P_{mn} \cos\left(\frac{2\pi m}{h} z\right) J_0\left(k_n \frac{\rho}{R}\right). \quad (\text{B7})$$

It should be noticed that contrast to Eq. (B6) the expansion (B7) contains the terms with

$$P_{0n} = \int_{-h/2}^{h/2} \frac{2d\tilde{z}}{h} \int_0^R \frac{2\tilde{\rho} d\tilde{\rho}}{R^2 J_1(k_n)^2} J_0\left(k_n \frac{\tilde{\rho}}{R}\right) P_Z(\tilde{\rho}, \tilde{z})$$

related to the average polarization

$$\langle P_Z(\rho, z) \rangle = \sum_{n=1}^{\infty} P_{0n} \frac{2J_1(k_n)}{k_n}.$$

The difference $P_Z(\rho, z) - \langle P_Z(\rho, z) \rangle$ acquires the form

$$P_Z(\rho, z) - \langle P_Z(\rho, z) \rangle = \sum_{m=1}^{\infty} \sum_{n=1}^{\infty} P_{mn} \cos\left(\frac{2\pi m}{h} z\right) J_0\left(k_n \frac{\rho}{R}\right) + \sum_{n=1}^{\infty} \left[J_0\left(k_n \frac{\rho}{R}\right) - \frac{2J_1(k_n)}{k_n} \right] P_{0n}. \quad (\text{B8})$$

Let us assume the good convergence of the series in Eqs. (A7) and (A8) and consider the particular following cases:

(1) In the particular case $h \ll \pi R$ one obtains that $\frac{1}{1+(k_n h/2\pi m R)^2} \approx 1$ at $n \leq m$ and

$$P_{mn} \approx \frac{2}{k_n J_1(k_n)} \int_{-h/2}^{h/2} \frac{2d\tilde{z}}{h} \cos\left(\frac{2\pi m}{h} \tilde{z}\right) P_Z(0, \tilde{z})$$

in accordance with Laplace method. Then we derive that the term

$$\sum_{n=1}^{\infty} \left[J_0\left(k_n \frac{\rho}{R}\right) - \frac{2J_1(k_n)}{k_n} \right] P_{0n} = 0$$

allowing for the unity expansion

$$1 = \sum_{n=1}^{\infty} \frac{2}{k_n J_1(k_n)} J_0\left(k_n \frac{\rho}{R}\right)$$

and equalities

$$1 \equiv \sum_{n=1}^{\infty} \frac{4}{k_n^2} \equiv \sum_{n=1}^{\infty} \frac{2}{k_n J_1(k_n)'},$$

which can be easily obtained from the unity expansion. Thus the approximate expression for depolarization field has the form [see Eqs. (B6)–(B8)]

$$E_Z^d(z) \approx -4\pi (P_Z(z) - \langle P_Z(z) \rangle). \quad (\text{B9})$$

Note, that Eq. (B9) is exact at $R \rightarrow \infty$ and coincides with the one obtained for ferroelectric films¹⁸ at $P_Z(\rho, z) \equiv P_Z(z)$.

(2) In the particular case $h \gg \pi R$ one obtains that $\frac{1}{1+(k_n h/2\pi m R)^2} \approx \left(\frac{2R}{h}\right)^2$ at $n \leq m$. Thus the depolarization field is rather small in comparison with Eq. (B9), namely,

$$|E_Z^d(\rho, z)| \sim 4\pi \left(\frac{2R}{h}\right)^2 [P_Z(z) - \langle P_Z(z) \rangle]. \quad (\text{B10})$$

The interpolation for the depolarization field that contains the aforementioned particular cases (B9) and (B10) acquires the form

$$E_Z^d(\rho, z) = -\frac{4\pi}{1+(h/2R)^2} (P_Z(z) - \langle P_Z(z) \rangle). \quad (\text{B11})$$

APPENDIX C

Variation of the free energy expressions (1)–(4) yields the following Euler-Lagrange equations with the boundary conditions on the cylinder butts $z = \pm h/2$, and the sidewall surface $\rho = R$ (see, e.g., Refs. 6 and 19)

$$\begin{cases} \alpha_R P_Z(\rho, z) + \beta P_Z^3(\rho, z) + \gamma P_Z^5(\rho, z) - \delta \left(\frac{\partial^2 P_Z(\rho, z)}{\partial z^2} + \frac{1}{\rho} \frac{\partial}{\partial \rho} \rho \frac{\partial}{\partial \rho} P_Z(\rho, z) \right) = E_0 + E_Z^d(\rho, z), \\ \left(P_Z + \lambda_b \frac{dP_Z}{dz} \right) \Big|_{z=h/2} = 0, \quad \left(P_Z - \lambda_b \frac{dP_Z}{dz} \right) \Big|_{z=-h/2} = 0, \quad \left(P_Z + \lambda_S \frac{dP_Z}{d\rho} \right) \Big|_{\rho=R} = 0, \end{cases} \quad (C1)$$

Let us find the approximate solution of the nonlinear Eq. (C1) by using the direct variational method as proposed earlier.¹⁹ Firstly we solved the linearized Eq. (C1)

$$P_Z(\rho, z) = \sum_{n=1}^{\infty} \frac{2J_0(k_n \rho/R)}{k_n J_1(k_n)} \left(\frac{E_0 + \eta \langle P_Z \rangle}{\alpha_R + \eta + \delta(k_n/R)^2} [1 - \varphi_n(z)] \right) \quad (C2)$$

$$\begin{cases} \varphi_n(z) = \frac{ch(\xi_n z)}{ch(\xi_n h/2) + \lambda_b \xi_n sh(\xi_n h/2)}, \\ \xi_n = \sqrt{(k_n/R)^2 + (\alpha_R + \eta)/\delta} \\ J_0(k_n) - (\lambda_S/R) k_n J_1(k_n) = 0 \end{cases} \quad (C3)$$

Here $J_0(k_n)$ and $J_1(k_n)$ are Bessel functions of the zero and first orders, respectively. In the general case the roots k_n depend over the ratio (λ_S/R) in accordance with Eq. (C3). Under the condition $(\lambda_S/R) \ll 1$ one obtains that $J_0(k_n) \approx 0$. For the case we used the Bessel functions norm $\langle J_0(k_n \rho/R) J_0(k_m \rho/R) \rangle = \delta_{nm} J_1^2(k_n)$ and equality $\langle J_0(k_m \rho/R) \rangle = 2J_1(k_m)/k_m$ in Eq. (C3).³¹

The average paraelectric polarization and dielectric permittivity acquire the form

$$\langle P_Z \rangle = \frac{\sum_{n=1}^{\infty} \frac{4}{k_n^2} \left(\frac{E_0(1 - \Phi_n)}{\alpha_R + \eta + \delta(k_n/R)^2} \right)}{1 - \eta \sum_{n=1}^{\infty} \left(\frac{4}{k_n^2} \cdot \frac{1 - \Phi_n}{\alpha_R + \eta + \delta(k_n/R)^2} \right)}, \quad (C4)$$

$$\langle \varepsilon_{zz} \rangle = \frac{d\langle P_Z \rangle}{dE_0} = \frac{4\pi \sum_{n=1}^{\infty} \frac{4}{k_n^2} \frac{(1 - \Phi_n)}{\alpha_R + \eta + \delta(k_n/R)^2}}{1 - \eta \sum_{n=1}^{\infty} \left(\frac{4}{k_n^2} \cdot \frac{1 - \Phi_n}{\alpha_R + \eta + \delta(k_n/R)^2} \right)}. \quad (C5)$$

Hereinafter $\langle \varphi_n(z) \rangle \equiv \Phi_n = \frac{2}{\xi_n h} \cdot \frac{sh(\xi_n h/2)}{ch(\xi_n h/2) + \lambda_b \xi_n sh(\xi_n h/2)}$.

The equation for paraelectric-ferroelectric phase transition temperature $T_{CN}(R, h)$ can be obtained from Eq. (C5) in the following form:

$$1 - \eta(R, h) \sum_{n=1}^{\infty} \frac{4}{k_n^2} \frac{1 - \Phi_n(R, h, T_{CN})}{\alpha_R(T_{CN}) + \eta(R, h) + \delta(k_n/R)^2} = 0. \quad (C6)$$

For a bulk sample $R \rightarrow \infty$, $h \rightarrow \infty$, and one obtains that $T_{CN}(R, h) \rightarrow T_C$ as it should be expected. For a nanodisk with

$R \gg h$ values $\eta \rightarrow 4\pi$ and $\xi_n \rightarrow \sqrt{4\pi/\delta}$, so the renormalized transition temperature acquires the form similar to the one derived in Ref. 20. For a nanowire with $h \rightarrow \infty$ values $\eta \rightarrow 0$ and $\langle \varphi(\xi_n) \rangle \sim 1/\xi_n h \rightarrow 0$, i.e., the depolarization field vanishes, thus $T_{CN}(R, h) \approx T_C - \frac{2\mu Q_{12}}{\alpha_T R} - \frac{k_1^2 \delta}{\alpha_T R^2}$. Intermediate situation is realized in prolate nanorods, when the inequality $h \gg R$ is valid, but the small values $\langle \varphi(\xi_n) \rangle \approx \frac{2}{(1 + \lambda_b \xi_n) \xi_n h}$ and $\eta(R, h) \approx 16\pi \cdot \frac{R^2}{h^2}$ are nonzero.

In particular case $\xi_n^2 \lambda_b h \gg 1$ we derived the interpolation for $T_{CN}(R, h)$ valid for the nanodisks, nanorods, and nanowires

$$T_{CN}(R, h) \approx T_C \left(1 - \frac{2\mu Q_{12}}{\alpha_T T_C R} - \frac{k_1^2 \delta}{\alpha_T T_C R^2} - \frac{2\eta(R, h)}{\alpha_T T_C (1 + \lambda_b \xi) \xi h} \right),$$

where

$$\xi(R, h) = \sqrt{\frac{1}{\delta} \left(\frac{k_1^2 \delta}{R^2} + \eta(R, h) \right)}, \quad k_1 \approx 2.405.$$

Really, using typical values $|\alpha| = 10^{-2}$, $\delta = 10^{-19} \text{ m}^2$, and $\lambda_b = 10^{-8} \text{ m}$, one can easily obtain that $\xi_n^2 \approx 4\pi/\delta$ and so $\xi_n^2 \lambda_b h \sim 10^2 - 10^3$ for the disks of height $h \sim 10^{-9} \text{ m}$ ($R \gg h$), whereas $\xi_n^2 \approx (k_n/R)^2 + \alpha/\delta \sim 10^{18} \text{ m}^{-2}$ and thus $\xi_n^2 \lambda_b h \sim 10^1 - 10^2$ for wires of radius $R \sim 10^{-9} \text{ m}$ ($h \gg R$).

Note, that the expression (C5) for paraelectric permittivity $\langle \varepsilon_{zz} \rangle$ coincides with one derived by Wang and Smith⁶ for the infinite cylinder at $(\lambda_S/R) \rightarrow 0$. In fact, for the case of infinite cylinder ($h \rightarrow \infty$) one can neglect the depolarization field ($\eta \rightarrow 0$) and dependence on z ($\varphi_n(z) \rightarrow 0$), so the summation on k_n leads to

$$\begin{aligned} P_Z(\rho, h \rightarrow \infty) &= E_0 \sum_{n=1}^{\infty} \frac{2J_0(k_n \rho/R)}{k_n J_1(k_n)} \frac{1}{\alpha_R + \delta(k_n/R)^2} \\ &= \frac{E_0}{-\alpha_R} \left(\frac{J_0(\rho \sqrt{-\alpha_R/\delta})}{J_0(R \sqrt{-\alpha_R/\delta})} - 1 \right), \end{aligned}$$

$$\begin{aligned} \langle P_Z \rangle &= E_0 \sum_{n=1}^{\infty} \frac{4}{k_n^2} \frac{1}{\alpha_R + \delta(k_n/R)^2} \\ &= \frac{E_0}{\alpha_R} \left(1 - \frac{2}{R \sqrt{-\alpha_R/\delta}} \frac{J_1(R \sqrt{-\alpha_R/\delta})}{J_0(R \sqrt{-\alpha_R/\delta})} \right). \end{aligned} \quad (C7)$$

In order to obtain the free energy with renormalized coefficients, let us use the coordinate-dependent part of the obtained solution in the trial function

$$P_Z(\rho, z) = \sum_{n=1}^{\infty} \frac{2J_0(k_n \rho/R) (1 - \varphi_n(z))}{k_n J_1(k_n)} P_n. \quad (\text{C8})$$

The variation amplitudes P_n must be determined by the minimization of the expressions (1)–(4). Integration in these expressions with the aforementioned trial function leads to the following form of the free energy:

$$\begin{aligned} \Delta G = & \frac{1}{2} \sum_{n=1}^{\infty} \frac{\alpha_R + \eta + \delta(k_n/R)^2}{1 - \Phi_n} \frac{4P_n^2}{k_n^2} - \frac{\eta}{2} \left(\sum_{n=1}^{\infty} \frac{4P_n}{k_n^2} \right)^2 \\ & - E_0 \sum_{n=1}^{\infty} \frac{4P_n}{k_n^2} + \frac{\beta}{4} \left(\sum_{l,n,s,q} g_{\text{lnsq}} P_l P_n P_s P_q \right) \\ & + \frac{\gamma}{6} \left(\sum_{l,n,s,q,r,t} f_{\text{lnsqrt}} P_l P_n P_s P_q P_r P_t \right). \quad (\text{C9}) \end{aligned}$$

The exact expressions for the renormalized coefficients in Eq. (C9) are rather cumbersome. Note, that hereinafter we suppose that $\xi_n^2 \lambda_b h \gg 1$ and so $\Phi_n \approx 2/h \xi_n (1 + \lambda_b \xi_n) \ll 1$, which is typical for the majority of ferroelectric nanoparticles.

The average polarization should be calculated as

$$\langle P_Z \rangle = \sum_{n=1}^{\infty} \frac{4P_n}{k_n^2}. \quad (\text{C10})$$

The coupled equations for the amplitudes P_n should be obtained from the variation $\frac{\partial \Delta G}{\partial P_n} = 0$.

*Electronic address: morozo@i.com.ua

†Electronic address: eliseev@i.com.ua

‡Electronic address: glin@materials.kiev.ua

- ¹D. Yadlovker and S. Berger, *Phys. Rev. B* **71**, 184112 (2005).
- ²G. Geneste, E. Bousquest, J. Junquera, and P. Chosez, *Appl. Phys. Lett.* **88**, 112906 (2006).
- ³Y. Luo, I. Szafraniak, N. D. Zakharov, V. Nagarajan, M. Steinhart, R. B. Wehrspohn, J. H. Wendroff, R. Ramesh, and M. Alexe, *Appl. Phys. Lett.* **83**, 440 (2003).
- ⁴F. D. Morrison, L. Ramsay, and J. F. Scott, *J. Phys.: Condens. Matter* **15**, L527 (2003).
- ⁵F. D. Morrison, Y. Luo, I. Szafraniak, V. Nagarajan, R. B. Wehrspohn, M. Steinhart, J. H. Wendroff, N. D. Zakharov, E. D. Mishina, K. A. Vorotilov, A. S. Sigov, S. Nakabayashi, M. Alexe, R. Ramesh, and J. F. Scot, cond-mat/0303609 (unpublished).
- ⁶C. L. Wang and S. R. P. Smith, *J. Phys.: Condens. Matter* **7**, 7163 (1995).
- ⁷I. Rychetsky and O. Hudak, *J. Phys.: Condens. Matter* **9**, 4955 (1997).
- ⁸D. D. Fong, G. B. Stephenson, S. K. Streiffer, J. A. Eastman, O. Auciello, P. H. Fuoss, and C. Thompson, *Science* **304**, 1650 (2004).
- ⁹S. K. Mishra and D. Pandey, *J. Phys.: Condens. Matter* **7**, 9287 (1995).
- ¹⁰K. Uchino, E. Sadanaga, and T. Hirose, *J. Am. Ceram. Soc.* **72**, 1555 (1989).
- ¹¹E. D. Mishina, K. A. Vorotilov, V. A. Vasiliev, A. S. Sigov, N. Ota, and S. Nakabayashi, *J. Exp. Theor. Phys.* **122**, 582 (2002).
- ¹²B. Jaffe, W. R. Cook, and H. Jaffe, *Piezoelectric Ceramics* (Academic Press, London, 1971).
- ¹³M. E. Lines and A. M. Glass, *Principles and Applications of Ferroelectrics and Related Phenomena* (Clarendon Press, Oxford, 1977).
- ¹⁴N. A. Pertsev, A. G. Zembilgotov, and A. K. Tagantsev, *Phys. Rev. Lett.* **80**, 1988 (1998).

- ¹⁵M. D. Glinchuk and A. N. Morozovska, *J. Phys.: Condens. Matter* **16**, 3517 (2004).
- ¹⁶D. R. Tilley, in *Ferroelectric Thin Films*, edited by C. Paz de Araujo, J. F. Scott, and G. W. Teylor (Gordon and Breach, Amsterdam, 1996), Chap. 2, pp. 11–45.
- ¹⁷L. D. Landau and E. M. Lifshits, *Electrodynamics of Continuous Media* (Butterworth Heinemann, Oxford, 1980).
- ¹⁸R. Kretschmer and K. Binder, *Phys. Rev. B* **20**, 1065 (1979).
- ¹⁹M. D. Glinchuk, E. A. Eliseev, and V. A. Stephanovich, *Physica B* **332**, 356 (2002).
- ²⁰M. D. Glinchuk and A. N. Morozovska, *Phys. Status Solidi B* **238**, 81 (2003).
- ²¹H. Huang, C. Q. Sun, Zh. Tianshu, and P. Hing, *Phys. Rev. B* **63**, 184112 (2001).
- ²²J. Freund, J. Halbritter, and J. K. H. Horber, *Microsc. Res. Tech.* **44**, 327 (1999).
- ²³G. A. Samara, *J. Phys.: Condens. Matter* **15**, R367 (2003).
- ²⁴F. Jona and G. Shirane, *Ferroelectric Crystals* (Pergamon Press, Oxford, 1962).
- ²⁵J. Zhang, Zh. Yin, M.-Sh. Zhang, and J. F. Scott, *Solid State Commun.* **118**, 241 (2001).
- ²⁶W. Ma, M. Zhang, and Z. Lu, *Phys. Status Solidi A* **166**, 811 (1998).
- ²⁷J. S. Speck and W. Pompe, *J. Appl. Phys.* **76**, 466 (1994).
- ²⁸R. Blinc and B. Zeks, *Soft Mode in Ferroelectrics and Antiferroelectrics* (North-Holland, Amsterdam, 1974).
- ²⁹Note, that for RS because of its monoclinic symmetry the coefficient $2Q_{12}$ in Eq. (14) should be substituted with $(Q_{12} + Q_{13})$, which can be found for instance in I. S. Zheludev, *Electrical Crystals* (Nauka, Moscow, 1979), in Russian.
- ³⁰A. I. Lurie, *Spatial Problems of the Elasticity Theory* (Gos. Izd. Teor. Tekh. Lit., Moscow, 1955), in Russian.
- ³¹H. Bateman and A. Erdelyi, *Higher Transcendental Functions*, Vol. 2 (McGraw-Hill, New York, 1953).